J. M. Serb, E. Sherratt, A. Alejandrino & D. C. Adams
Phylogenetic convergence and multiple shell shape optima for gliding scallops (Bivalvia: Pectinidae)
Journal of Evolutionary Biology, 2017; 30(9):1736-1747

Phylogenetic convergence and multiple shell shape optima for gliding scallops (Bivalvia: Pectinidae)

Journal:	*Journal of Evolutionary Biology*
Manuscript ID	JEB-2017-00260
Manuscript Type:	Research Papers
Keywords:	Morphometrics, macroevolution, Mollusca, Morphology, Phylogenetics

Abstract

An important question in evolutionary biology is how often, and to what extent, similar ecologies elicit the same phenotypic response in distantly related taxa. In some scenarios, the repeated evolution of particular phenotypes may be expected, for instance when species are exposed to common selective forces that result from strong functional demands. In bivalved scallops (Pectinidae), some species exhibit a distinct swimming behavior (gliding), which requires specific biomechanical attributes to generate lift and reduce drag during locomotive events. Further, a phylogenetic analysis revealed that gliding behavior has independently evolved at least four times, which raises the question as to whether these independent lineages have also converged on a similar phenotype. In this study, we test the hypothesis that gliding scallops display shell shape convergence using a combination of geometric morphometrics and phylogenetic comparative methods that evaluate patterns of multivariate trait evolution. Our findings reveal that the gliding species display less morphological disparity and significant evolutionary convergence in morphospace, relative to expectations under a neutral model of Brownian motion for evolutionary phenotypic change. Intriguingly, the phylomorphospace patterns indicate that gliding lineages follow similar evolutionary trajectories to not one, but two regions of morphological space, and subsequent analyses identified significant differences in their biomechanical parameters, suggesting that these two groups of scallops accomplish gliding in different ways. Thus, while there is a clear gliding morphotype that has evolved convergently across the phylogeny, functionally distinct morphological sub-forms are apparent, suggesting that there may be two optima for the gliding phenotype in the Pectinidae.

Introduction

How often, and to what extent, do similar ecologies elicit the same phenotypic response in distantly related taxa? Alike phenotypes can arise when species exploit a common trophic niche and evolutionarily respond in a congruent manner to those selective constraints required for particular function or biomechanical task (Herrel *et al.*, 2008; Vincent *et al.*, 2009; Adams & Nistri, 2010). This is the pattern of convergence, the repeated evolution of similar traits among multiple lineages that ancestrally lack the trait (Stayton, 2015), and convergent evolution is regularly treated as evidence for adaptation (Harvey & Pagel, 1991; Larson & Losos, 1996). Some of the best known examples of convergent evolution are seen in the similarity in body plans of the succulent plants in Euphorbiaceae and Cactaceae (Alvarado-Cárdenas *et al.*, 2013) and Old and New World anteaters (Beck *et al.*, 2006), or the similarity of skull shape between the marsupial Thylacine (Tasmanian wolf) and that of the placental canids (Wroe & Milne, 2007; Goswami *et al.*, 2011).

However, convergence need not create perfect morphological replicas. Rather, there can be varying degrees of morphological variance among phenotypes even if they experience selective regimes that impose similar or identical functional demands. For example, lineages may converge towards a general area of morphospace, but occupy different regions within it (Herrel *et al*., 2004; Leal *et al*., 2002; Stayton, 2006). Likewise, independent lineages may evolve to a distinct region in morphospace, but the size of this region may be larger than what the morphospace is for the ancestral phenotypes of those lineages (Collar *et al*., 2014). Furthermore, when multiple levels of biological organization are compared, one may observe convergence in the ability to perform a particular task across a set of taxa, even when such taxa exhibit distinct or even divergent morphologies (reviewed in Wainwright, 2007). This disconnect across the functional-morphological boundary can occur when modular morphological components are

present, allowing for distinct combinations of morphological forms to create similar functional properties ('many-to-one mapping' of form to function: Alfaro *et al*., 2004; Wainwright *et al*., 2005).

For evolutionary biologists, quantifying convergent patterns has long been an analytical challenge, and numerous approaches have been suggested to characterize particular attributes that inform on patterns and processes of convergence (Stayton, 2006, 2008; Muschick *et al.*, 2012; Arbuckle *et al.*, 2014). However, several recently-developed synthetic quantitative measures have been proposed which characterize the overall extent to which two or more lineages display convergent morphological patterns (Stayton, 2015). Importantly, these approaches are process-neutral; describing only patterns of convergence, and leveraging the shared phylogenetic history of the taxa under investigation when making evolutionary inferences of those patterns (see Stayton, 2015). As such, these tools provide a powerful means of evaluating evolutionary convergence, and provide key evidence in determining the extent to which independent lineages converge on a common phenotype or display a suite of closely related solutions to similar ecological challenges.

One the strongest illustrations for how functional demands influence morphology is the many instances of convergent shell form of bivalved molluscs (Bivalvia). It has long been recognized that there is a strong association between shell form and ecological niche in bivalves (Verrill, 1897; Kauffman, 1969; Stanley, 1970, 1972). Stanley (1970) was the first to described in detail how particular shell traits are found in species belonging to one of seven "life habit" classes (*sensu* Stanley, 1970), which are defined by the animal's life position relative to the substrate, type of locomotion or attachment, and feeding mode (hereafter referred to as "ecomorphs" *sensu* Williams, 1972). Thus, shell form is the evolutionary response to the external

requirements for living space, locomotion, defense, and survival of the adult animal. Modifications to shell morphology include changes to the overall outline of each valve (left vs. right), the form along the hinge, the degree of shell inflatedness (convexity vs. concavity), or the extent of ornamentation over each valve. In ecological classes with more specific performance needs, there is a greater opportunity for convergent shell forms (Stanley, 1972; Thomas, 1978; Serb *et al.*, 2011). Thus, performance may be a strong predictor of the degree of shell shape convergence.

Within scallops (Bivalvia: Pectinidae), one striking example of convergent evolution is found in species displaying high-performance swimming, or gliding, behavior (Serb *et al.*, 2011; Mynhardt *et al.*, 2015). This behavior is characterized by the expulsion of water from the mantle cavity while the valves are closed, allowing the animal to propel forward with the ventral-edge leading (Manuel & Dadswell, 1993; Cheng *et al.*, 1996). The biomechanic properities of gliding have been extensively studied, and we have a good understanding of the parameters important to maximize performance (Morton, 1980; Joll, 1989; Hayami, 1991; Millward & Whyte, 1992; Manuel & Dadswell, 1993; Cheng *et al.*, 1996; Ansell *et al.*, 1998; Himmelman *et al.*, 2009; Guderley & Tremblay, 2013; Tremblay *et al.*, 2015). Intriguingly, some measurements of gliding kinematics vary within the ecomorph (Caddy, 1968; Morton, 1980; Joll, 1989; Ansell *et al.*, 1998; Mason *et al.*, 2014), suggesting that there are differences among the functional components of locomotion (see results below). However, it is unknown whether these differences are the result of variation in shell shape, or other functionally-relevant morphological traits (Guderley & Tremblay, 2013). Collectively, species in the gliding ecomorph have a qualitatively similar shell form that is discoid in shape, lacks prominent external shell surface sculpture, and have a left valve that is slightly more convex than the lower right valve (Stanley,

1970; Gould, 1971). In this instance where there appears to be a tight association between shell shape and performance, the morphology would be predicted to be under strong selection, resulting in a narrow area of occupied morphospace for gliding lineages.

Interestingly, the phylogenetic history of the gliding form across the Pectinidae is uncertain, but a recent phylogenetic analysis revealed that the behavior has evolved independently in at least four lineages: *Adamusium-Placopecten*, *Amusium*, *Euvola*, and *Ylistrum* (Alejandrino *et al*., 2011). Previous work (Serb *et al.*, 2011) has shown that morphological similarities in shell shape occur between two gliding lineages (*Amusium* and *Ylistrum*; Fig 1b-d), but at the time a more comprehensive phylogenetic framework, as well as the necessary analytical tools (*sensu* Stayton, 2015), were lacking to rigorously test the hypothesis of more widespread morphological convergence in the group. In this study, we test the hypothesis that shell shape similarity in gliding scallops is the result of evolutionary convergence, using expanded taxon sampling which includes all five genera with gliding species. We adopt an integrative approach combining 3-D geometric morphometric techniques to quantify shell shape variation and phylogenetic comparative methods to infer the history of morphological diversification across species. With this approach we test the following hypotheses: 1) the specific biomechanic requirements of gliding have led to morphological convergence in shell shape; 2) due to the the importance of shell shape for efficient gliding, the shell morphologies of gliding species will exhibit less shell shape variation, and taxa will therefore occupy a more restricted region of morphospac, than non-gliding ecomorphs; and 3) differences in shell shape are related to differences in how gliding is performed biomechanically, potentially resulting in multiple anatomical solutions for a common biomechanical challenge. To quantitatively address these hypotheses, we utilize phylogenetic comparative methods for evaluating trends in high-

dimensional multivariate data (Adams, 2014a; b), new methods for evaluating morphological disparity in a phylogenetic context, as well as several recently-developed measures that evaluate the degree of evolutionary convergence relative to what is expected based on the phylogeny for the group (Stayton, 2015). Our findings reveal strong evidence for evolutionary convergence in shell shape of gliding species, in which gliding lineages follow similar trajectories to not one, but two regions of morphological space. This pattern suggests that there may be two optima for the gliding phenotype in the Pectinidae.

Materials and Methods

Specimen selection and morphological characterization: A total of 933 specimens from 121 species were used in this study, and were selected to represent a wide range of taxa displaying all six ecomorphs exhibited in the Pectinidae (data from Sherratt *et al.*, 2016) (natural history museums listed in Table S1 and Acknowledgments. For each specimen, shell morphology was quantified using geometric morphometric methods (Bookstein, 1991; Mitteroecker & Gunz, 2009; Adams *et al.*, 2013). These methods utilize the locations of landmark coordinates as the basis of shell shape quantification. The method is identical to Sherratt *et al*. (2016), and uses a total of 202 landmarks and semilandmarks to characterize shell shape (Fig. 1). Briefly, we first obtained high-resolution scans of the left valves of each individual using a NextEngine 3D surface scanner. From these scans we then digitized the locations of five homologous anatomical locations following Serb *et al*. (2011): 1: ventroposterior auricle, 2: dorsoposterior auricle, 3: umbo, 4: dorsoanterior auricle, 5: ventroanterior auricle (Fig. 1). Next, twelve semilandmarks were placed equidistantly between these fixed points to capture the shape of the auricles, and 35 equidistant points were placed along the ventral edge of the valve between the anterior and posterior auricles. Finally, we used an automated procedure to fit 150 semi-landmarks to the

144 shell surface using a template; these are allowed to slide in 3D over the surface (Gunz *et al.*,
145 2005; Serb *et al.*, 2011; Sherratt *et al.*, 2016).
146 To obtain a set of shape variables for each specimen, we aligned the 933 landmark
147 configurations using a generalized Procrustes analysis (GPA: Rohlf & Slice, 1990). Procrustes
148 superimposition removes differences in specimen position, orientation, and scale, and aligns all
149 specimens to a common coordinate system. During this analysis, the semilandmarks were
150 permitted to slide along their tangent directions using the Procrustes distance criterion. The
151 aligned specimens were then projected orthogonally to tangent space to obtain a set of shape
152 variables (Procrustes tangent coordinates: Rohlf, 1990) for use in all subsequent analyses.
153 Specimen digitizing and GPA were performed in R 3.3.2 (R Core Team, 2017) using the package
154 *geomorph* v.3.0.3 (Adams & Otárola-Castillo, 2013; Adams *et al.*, 2016).
155 *Statistical Analyses*: Overall patterns of variation in shell shape were visualized in
156 morphospace using a principal components analysis (PCA). However, because species are not
157 independent of one another, all subsequent statistical analyses evaluating our evolutionary
158 hypotheses were conducted on species means and using a phylogenetic comparative framework.
159 To evaluate morphological trends in a phylogenetic context, we performed several phylogenetic
160 comparative analyses, using a multi-gene molecular phylogeny containing 143 species of
161 Pectinidae (Fig. S1; Table S2) (Alejandrino *et al*,. 2011; Sherratt *et al*., 2016). Briefly, we
162 constructed a robust, time-calibrated phylogeny using sequence data from two mitochondrial
163 genes (12S, 16S ribosomal RNAs) and two nuclear genes (histone H3, 28S ribosomal RNA)
164 which were obtained from museum specimens using procedures in Puslednik and Serb (2008)
165 and Alejandrino *et al*. (2011). Sequence data were aligned using CLUSTAL W (Thompson *et al.*,
166 1994) in Geneious Pro v.5.6.4 (http://www.geneious.com) (Kearse *et al.*, 2012) with a gap-

opening penalty of 10.00 and a gap-extending penalty of 0.20. GBlocks Server (Talavera & Castresana, 2007) was used to remove ambiguous alignment in 16S rRNA. For Bayesian inference, we used a relaxed clock model as implemented in BEAST v.1.8.0 (Drummond & Rambaut, 2007) with a speciation model that followed incomplete sampling under a birth-death prior and rate variation across branches uncorrelated and exponentially distributed. Three independent simulations of Markov Chain Monte Carlo for 20 million generations were run, sampling every 100 generations, and 20,000 trees were discarded as burn-in using Tracer v.1.6 l (Rambaut *et al.*, 2014). The remaining trees were combined in LogCombiner; the best tree was selected using TreeAnnotator. We used 30 fossils to constrain the age of nodes through assigning node priors, details of which are in Sherratt *et al.* (Table 2 in 2016).

Combining the morphological and phylogenetic data, the mean shell shape was estimated for each species and the morphological dataset was matched to the phylogeny. As there were 93 species shared between the two datasets, and the phylogeny and the morphological data matrix were pruned to contained the unique set of 93 taxa (Fig. 2, as in Sherratt *et al*. 2016). Phylogenetic patterns of shell shape evolution were examined using several approaches. First, to evaluate phylogenetic trends in the shape data we first conducted an analysis of phylogenetic signal, using the multivariate version of the *kappa* statistic (K_{mult}: (Adams, 2014a). Next, we performed a phylogenetic analysis of variance (ANOVA) to evaluate whether shell shape differed among ecomorphs while accounting for phylogenetic non-independence. This approach is based on a generalization of phylogenetic generalized least squares (PGLS), and is appropriate for evaluating trends in high-dimensional multivariate data (described in Adams, 2014; Adams & Collyer, 2015). We visualized patterns of shell shape evolution using a phylomorphospace approach (*sensu* Sidlauskas, 2008), where the extant taxa and the phylogeny were projected into

morphospace, and evolutionary changes in shape were visualized along the first two axes of this space using PCA.

Finally, we performed several quantitative analyses to evaluate the degree of morphological convergence in a phylogenetic context, including two recently-developed convergence measures (Stayton, 2015). The first convergence measure, C_1 (Stayton, 2015), characterizes the degree of morphological difference between extant taxa relative to the maximal morphological distance between any of their ancestors. This measure represents the proportion of morphological divergence that has been reduced in the extant taxa, with a maximal value (1.0) indicating the extant species are morphologically identical (Stayton, 2015). The second convergence measure, C_5 (Stayton, 2015), describes the frequency of convergence into a particular region of morphospace, and is estimated by determining the number of extant lineages of the putatively convergent taxa that cross the boundary of a convex hull formed by the focal taxa (Stayton, 2015). Both measures were statistically evaluated using phylogenetic simulation, where multivariate datasets are simulated along the phylogeny using Brownian motion, and the observed test measures are compared to a distribution of possible values obtained from these simulations to assess their significance (Stayton, 2015).

Additionally, we evaluated whether the degree of morphological disparity (Stayton, 2006; see also Zelditch *et al.*, 2012) among species in the gliding ecomorph was less than expected by chance while accounting for phylogenetic relatedness using two novel approaches. For the first approach, we estimated the observed morphological disparity among species within each ecomorph, and ranked the degree of disparity in the gliding ecomorph relative to the disparity observed within all other ecomorphs. Then, we generated 1000 simulated datasets under a Brownian motion model of evolution, using the time-dated molecular phylogeny above and an

input covariance matrix based on the covariance matrix of the observed shape data. From each dataset, we then estimated measures of morphological disparity for each ecomorph, and compared the observed patterns of disparity to what was expected under a Brownian motion model of evolution (for a related procedure see: Garland Jr. *et al.*, 1993; Sherratt *et al.*, 2016).

Our second approach accounted for the phylogeny directly in the disparity calculations. Here, we performed a transformation of the data using the phylogenetic transformation matrix (Garland, Jr., & Ives, 2000; see also Adams, 2014b), and obtained estimates of disparity for each ecomorph in the phylogenetically-transformed space following standard computations. The phylogenetic morphological disparity for the gliding ecomorph was then evaluated statistically using permutation tests, where morphological values were permuted across the tips of the phylogeny to disassociate the morphological data from the ecomorph groups (see Adams, 2014a). Note that our procedure for phylogenetic morphological disparity differ from that of Brusatte *et al*. (2017), in that our approach directly accounts for species' non-independence due to the phylogeny when estimating patterns of morphological diversity in extant taxa. By contrast, Brusatte *et al.* (2017) use estimated ancestral states to inform disparity measures among fossils at particular time periods in the paleontological history of a group, but did not incorporate the phylogeny in extant analyses directly. All analyses were performed in R 3.3.2 (R Core Team, 2017) using the package *geiger* 2.0.6 (Pennel *et al.*, 2014), the package *geomorph* v.3.0.3 (Adams & Otárola-Castillo, 2013; Adams *et al.*, 2016), the package *convevol* v.1.0 (Stayton, 2014), and routines written by one of the authors (DCA).

Biomechanical data and analysis: In addition to morphological data we obtained several measurements of functional performance in swimming for four species of gliding scallops (*A. pleuronectes, Ad. colbecki, P. magellanicus,* and *Y. balloti*). Performance measures were taken

from the primary literature, and were based on swimming trials of animals in the laboratory (Morton, 1980) or under natural conditions (Joll, 1989; Ansell *et al.*, 1998; Mason *et al.*, 2014). Data collected by SCUBA divers and high-definition video recordings include: distance traveled, the number of adductions during the swimming bout, swimming time, and swimming velocity. Because data from some publications were presented only as means and standard deviations, we performed t-tests comparing pairs of taxa for each performance measure.

Results

Visual inspection of morphospace using PCA revealed distinct clusters that broadly corresponded to the ecomorph groups (Fig. 3). Specifically, the free-living and byssal attaching ecomorphs occupied most of the morphospace and overlapped greatly in PC1 vs PC2, but showed some separation along PC3. The recesser ecomorph formed an elongate cluster extending away from the main cloud of free/byssal species. The specimens of *Pedum spondyloideum*, the only nestling species, were all very different from one another, and lay at the edge of the free-living/byssal attaching ecomorph cloud, as did species of the cementing ecomorph (see full list in Supplementary Materials, Table S1).

The gliding ecomorph occupies the extreme positive end of PC2 where valves have smaller auricles compared to other ecomorphs. Interestingly, these gliding individuals occupied two distinct regions of morphospace. This implies that two sub-clusters of similar, yet subtly distinct shell shapes were exhibited by species that utilize this behavior. The shape difference between the two gliding morphotypes was described by the degree of valve flatness (Z-axis), where flatter valves were at the positive end of PC1 (Fig. 3, lateral views). Further, gliding species appeared to display less variation in shell shape when compared to the other ecomorphs,

as the patterns of distribution in morphospace of the two clusters were each more restricted compared to other ecomorphs.

Across scallops, shell shape displayed significant phylogenetic sigal (K_{mult} = 0.2778; P <0.001). Using phylogenetic ANOVA, we found significant differences in shell shape across ecomorphs (D-PGLS, $F_{5,87}$ = 5.505, P < 0.001, R^2 = 0.240, Z = 8.60), implying that the functional groups were morphologically distinct in spite of shared evolutionary history. When viewed in phylomorphospace (Fig. 4), the shell shape differences were evident, with the gliding species occupying a unique region of morphospace when compared to taxa from the other functional groups. Lending support to this visual observation, both measures of convergence for the gliding taxa revealed strong evolutionary signals for morphological similarity in gliding species. Specifically, the average measure C_1 between pairs of gliding taxa was 0.45, indicating that the extant gliding species occupied 45% less of morphospace as compared to the maximum spread of their ancestors. Using Brownian motion simuations, this value was highly significant (P > 0.001). Likewise, the number of convergent events in gliding species (C_5 = 5) was significantly greater than would be expected from a Brownian motion model of evolution (P = 0.016). Additionally, gliding species displayed the lowest levels of within-ecomorph disparity (Table 1), and this pattern differed significantly from what was expected under a Brownian motion model of evolution (P = 0.031). Further, when morphological disparity was evaluated in a phylogenetic context, there was less variation within the gliding ecomorph than expected by a random association of morphology and ecotype ($MD_{glide} = 3.28 \times 10^{-5}$; P = 0.004: Table 1). Taken together, these analyses provided significant empirical support for the hypothesis that species in the gliding ecomorph displayed phylogenetic evolutionary convergence.

Interestingly, as was observed in the PCA of all individuals, phylogenetic patterns in shell shape viewed in phylomorphospace (Fig. 4) revealed two clear clusters of gliding species. One of these clusters (the 'A' morphotype) was comprised of four species derived from three distinct phylogenetic lineages [*Ylistrum ballotti* (Bernardi, 1861) & *Y. japonicum* (Gmelin, 1791); *Amusium pleuronectes* (Linnaeus, 1758); *Euvola papyraceum* Gabb, 1873] (species d, c, b, and a, respectively, in Fig. 2) (Pectininae; see Serb, 2016). The 'B' gliding morphotype was comprised of species from two Tribes [Adamussiini: *Adamussium colbecki* (Smith, 1902) & Palliolini: *Placopecten magellanicus* (Gmelin, 1791)] (Serb, 2016) (species e and f: Fig. 2). Thus, patterns of phenotypic evolution of shell shape appeared to display two distinct gliding morphologies. Interestingly, we observed significant differences in biomechanical performance measures between species in these two morphotypes, with the A morphotype attaining greater distances, displaying a higher number of adductions, longer swim times, and faster velocities then the B morphotype (Table 3). Taken together, these results imply that there are two two gliding morphs in scallops, and each has accomplished their gliding behavior differently from a biomechanical perspective.

Discussion

Morphological convergence provides a series of independent tests of the phenoptypic response to a particular selective regime. In phenotypes where performance level is determined by the morphology of the organism, strong selective forces may act on specific components of that form. In the case of gliding scallop species, this hypothesis is supported. Specifically, we found significant similarity in shell shape across these species in a manner suggestive of evolutionary convergence. Further, explicit tests of evolutionary convergence revealed that the

observed similarities were unlikely if traits evolved under multivariate Brownian motion, lending additional support to the convergence hypothesis. Together our results are consistent with the prediction that locomotory performance elicits selection on shell morphology, resulting in evolutionary convergence in shell shape in those species which have independently evolved gliding behavior. Interestingly, while gliding taxa do occupy a distinct region in morphospace from scallop species exhibiting other behaviors, the evolution of the gliding form in Pectinidae is not a simple example of convergence. Rather, there is still some additional structure within the gliding morphotype suggestive of both overall convergence in shell shape, as well as a degree morphological divergence (a relatively flat valve with small auricles, and the degree of valve flatness, respectively). This latter finding is evidenced by the fact that two clusters of gliding taxa are evident in phylomorphospace (Fig. 4; see also Fig. 3), and that species in these two clusters display significant differences in biomechanical performance (Table 3). Thus, while there is a clear gliding morphotype displayed across all gliding lineages, sub-forms within this group are also apparent.

From these observations, we can draw three conclusions. First, morphological convergence in shell shape does occur for the five gliding lineages, and lineages occur in a distinct, but broad, region of morphospace, separate from other life habit forms. Second, while all gliding species occupy the same general region of morphospace, among the gliders, two morphotypes can be distinguished. This implies that two subtle, yet distinct shell shapes are exhibited by species that must solve the same performance challenges related to the gliding behavior. Third, gliding has more restrictive shell form requirements than other life habits. Gliding species display less variation in shell shape when compared to the other life habits. Indeed, the two gliding morphotypes had roughly 30% of the variation observed in the other life

habit groups, indicating a significant reduction in shell shape variation among gliding individuals. Overall, both the individual-based patterns (Fig. 3) and the phylomorphospace pattern (Fig. 4) suggest that there may be two optima for the gliding phenotype in the Pectinidae.

Interestingly, the limited performance data on gliding in scallops is consistent with our two optima hypothesis implied by the morphological data. Several parameters of functional performance in swimming have been evaluated in these taxa, and slight differences in these biomechanical parameters exist between the gliding species including: the maximum distance traveled of a single swim, the number of adductions per swimming effort, and horizontal swimming speed (Caddy, 1968; Morton, 1980; Joll, 1989; Ansell *et al.*, 1998) (Table 2). Further, the differences in performance observed between taxa also correspond to the two gliding morphotypes found in this study. When placed in the context of our morphological findings, it is clear that the two gliding morphotype differ in how they locomote. Specifically, the data examined here suggest that members of morphotype A (*A. pleuronectes, E. papyraceum, Y. balloti,* and *Y. japonicum)* can swim faster and for longer distances than members of morphotype B (*P. magellanicus, Ad. colbecki*) (Tables 2-3). We hypothesize this may be a direct result of a more effective gliding phase due to shells having a more discoid and aerodynamic form through the reduction of the auricles (and other conclusions from our results). This hypothesis has support from previous work by Hayami (1991), who found *Y. japonicum* (morphotype A) shells have the lower value of drag coefficient and higher lift-drag ratio when compared to *P. magellanicus* (morphotype B), which is likely to be because morphotype A is flatter than B. Future biomechanical studies directly linking gliding performance with three-dimensional shell shape would be essential in testing these observations and this hypothesis.

A central conclusion of our study is that the shell shape of gliding scallops exhibits a strong pattern of convergence. Quantifying convergence is important not only for identifying major evolutionary trends, but to discover, and subsequently measure, the more subtle degrees of morphological convergence. This variation can then be placed into the relevant biological context and direct future research efforts. However, the challenge has been to apply a pattern-based, rather than process-based, approach. The recent development of quantative, pattern-based evolutionary convergence tests finally provides us with a useful set of tools to evaluate convergence within a phylogenetic context (Stayton, 2015). This approach has been used successfully to quantify convergent evolution across ecological guilds in a wide variety of taxa including pythons and boas (Esquerré *et al.*, 2016), planktivorous surgeonfishes (Friedman *et al.*, 2016), social swallows (Johnson *et al.*, 2016) and squirrels (Zelditch *et al.*, 2017). Thus, the application of quantitative measures should illuminate convergence patterns in understudied taxa and provide key evidence in determining the extent to which independent lineages converge on a common phenotype or display a suite of closely related solutions to similar ecological challenges.

References

Adams, D. 2014a. A generalized K statistic for estimating phylogenetic signal from shape and other high-dimensional multivariate data. *Syst. Biol.* **63**: 685–697.

Adams, D. 2014b. A method for assessing phylogenetic least squares models for shape and other high-dimensional multivariate data. *Evolution (N. Y).* **68**: 2675–2688.

Adams, D. & Otárola-Castillo, E. 2013. geomorph: an R package for the collection and analysis of geometric morphmetric shape data. *Methods Ecol. Evol.* **4**: 393–399.

374 Adams, D., Rohlf, F.J. & Slice, D.E. 2013. A field comes of age: Geometric morphometrics in
375 the 21st century. *Hystrix* **24**: 7–14.
376 Adams, D.C. & Collyer, M.L. 2015. Permutation tests for phylogenetic comparative analyses of
377 high-dimensional shape data: What you shuffle matters. *Evolution (N. Y).* **69**: 823–829.
378 Adams, D.C., Collyer, M.L., Kaliontzopoulou, A. & Sherratt, E. 2016. geomorph 3.0.3: software
379 for geometric morphometric analyses.
380 Adams, D.C. & Nistri, A. 2010. Ontogenetic convergence and evolution of foot morphology in
381 European cave salamanders (Family: Plethodontidae). *BMC Evol. Biol.* **10**: 1–10.
382 Alejandrino, A., Puslednik, L. & Serb, J.M. 2011. Convergent and parallel evolution in life habit
383 of the scallops (Bivalvia: Pectinidae). *BMC Evol. Biol.* **11**: 164.
384 Alfaro, M.E., Bolnick, D.I. & Wainwright, P.C. 2004. Evolutionary dynamics of complex
385 biomechanical systems: an example using the four-bar mechanism. *Evolution* **58**: 495–503.
386 Alvarado-Cárdenas, L.O., Martínez-Meyer, E., Feria, T.P., Eguiarte, L.E., Hernández, H.M.,
387 Midgley, G., *et al.* 2013. To converge or not to converge in environmental space: Testing
388 for similar environments between analogous succulent plants of North America and Africa.
389 *Ann. Bot.* **111**: 1125–1138.
390 Ansell, A.D., Cattaneo-Vietti, R. & Chiantore, M. 1998. Swimming in the Antartic scallop
391 Adamussium colbecki analysis of in situ video recordings. *Antarct. Sci.* **10**: 369–375.
392 Arbuckle, K., Bennett, C. & Speed, M. 2014. A simple measure of the strength of convergent
393 evolution. *Methods Ecol. Evol.* **5**: 685–693.
394 Beck, R.M.D., Bininda-Emonds, O.R.P., Cardillo, M., Liu, F.-G.R. & Purvis, A. 2006. A higher-
395 level MRP supertree of placental mammals. *BMC Evol. Biol.* **6**: 93.
396 Bernardi, C. 1861. *Journal de Conchyliologie.* P.-H. Fischer., [Paris].
397 Bookstein, F.L. 1991. *Morphometric tools for landmark data: geometry and biology*. Cambridge
398 University Press, Cambridge.
399 Brusatte, S.L., Montanair, H.-Y. & Norell, M. 2017. Phylogenetic corrections for morphological
400 disparity analysis: new methodology and case studies. *Paleobiology* **37**: 1–22.
401 Caddy, J.F. 1968. Underwater observations on scallop (Placopecten magellanicus) behavior and
402 drag efficiency. *J. Fish. Res. Board Canada* **25**: 2123–2141.
403 Cheng, J., Davison, I.G., Demont, M.E. & Chang, J.-Y. 1996. Dynamics and energetics of
404 scallop locomotion. *J. Exp. Biol.* **199**: 1931–1946.

Collar, D.C., Reece, J.S., Alfaro, M.E., Wainwright, P.C. & Mehta, R.S. 2014. Imperfect morphological convergence: variable changes in cranial structures underlie transitions to durophagy in moray eels. *Am. Nat.* **183**: E168-84.

Drummond, A.J. & Rambaut, A. 2007. BEAST: Bayesian evolutionary analysis by somping trees. *BMC Evol. Biol.* **7**: 214.

Esquerré, D., Scott Keogh, J. & Harmon, L. 2016. Parallel selective pressures drive convergent diversification of phenotypes in pythons and boas. *Ecol. Lett.* **19**: 800–809.

Friedman, S.T., Price, S.A., Hoey, A.S. & Wainwright, P.C. 2016. Ecomorphological convergence in planktivorous surgeonfishes. *J. Evol. Biol.* **29**: 965–978.

Garland, Jr., T. & Ives, A.R. 2000. Using the past to predict the present: Confidence intervals for regression equations in phylogenetic comparative methods. *Am. Nat.* **155**: 346–364.

Garland Jr., T., Dickerman, A.W., Janis, C.M. & Jones, J.A. 1993. Phylogenetic analysis of covariance by computer simulation. *Syst. Biol.* **42**: 265–292.

Gmelin, J.F. 1791. *Caroli a Linné, systema naturae. Tom. I. Pars VI.* Lipsiae [Leipzig] :

Goswami, A., Milne, N. & Wroe, S. 2011. Biting through constraints: cranial morphology, disparity and convergence across living and fossil carnivorous mammals. *Proc. Biol. Sci.* **278**: 1831–1839.

Gould, S.J. 1971. Muscular mechanics and the ontogeny of swimming in scallops. *Palaeontology* **14**: 61–94.

Guderley, H.E. & Tremblay, I. 2013. Escape responses by jet propulsion in scallops. *Can. J. Zool.* **91**: 420–430.

Gunz, P., Mitteroecker, P. & Bookstein, F.L. 2005. Semilandmarks in three dimensions. In: *Modern morphometrics in physical anthropology* (D. E. Slice, ed), pp. 73–98. Klewer Academic/Plenum Publishers, New York.

Harvey, P.H. & Pagel, M.D. 1991. *The comparative method in evolutionary biology*. Oxford University Press, Oxford.

Hayami, I. 1991. Living and fossil scallop shells as airfoils: an experimental study. *Paleobiology* **17**: 1–18.

Herrel, A., Vanhooydonck, B. & Van Damme, R. 2004. Omnivory in lacertid lizards: Adaptive evolution or constraint? *J. Evol. Biol.* **17**: 974–984.

Herrel, A., Vincent, S.E., Alfaro, M.E., Wassenbergh, S. Van, Vanhooydonck, B. & Irschick,

D.J. 2008. Morphological convergence as a consequence of extreme functional demands: examples from the feeding system of natricine snakes. *J. Evol. Biol.* **21**: 1438–1448.

Himmelman, J.H., Guderley, H.E. & Duncan, P.F. 2009. Responses of the saucer scallop Amusium balloti to potential predators. *J. Exp. Mar. Bio. Ecol.* **378**: 58–61.

Johnson, A.E., Mitchell, J.S. & Brown, M.B. 2016. Convergent evolution in social swallows (Aves: Hirundinidae). *Ecol. Evol.* 550–560.

Joll, L.M. 1989. Swimming behavior of the saucer scallop Amusium balloti (Mollusca, Pectinidae). *Mar. Biol.* **102**: 299–305.

Kauffman, E.G. 1969. Form, function, and evolution. In: *Treatis on Invertebrate Paleontology, Part N, Mollusca 6, Bivalvia* (R. C. Moore, ed), pp. N130–N205. Geological Society of American and University of Kansas, Lawrence, KS.

Kearse, M., Moir, R., Wilson, A., Stones-Havas, S., Cheung, M., Sturrock, S., *et al.* 2012. Geneious Basic: An integrated and extendable desktop software platform for the organization and analysis of sequence data. *Bioinformatics* **28**: 1647–1649.

Larson, A. & Losos, J.B. 1996. Phylogenetic systematics of adaptation. In: *Adaptation* (M. R. Rose & G. V Lauder, eds), pp. 187–220. Academic Press, San Diego.

Leal, M., Knox, A.K. & Losos, J.B. 2002. Lack of convergence in aquatic Anolis lizards. *Evolution* **56**: 785–791.

Linnaeus, C. 1758. *Systema Naturae per Regna tria naturae, secundum classes, ordines, genera, species, cum characteribus, differentiis, synonymis, locis [...] Tomus I, Editio Decima, Reformata*.

Manuel, J.L. & Dadswell, M.J. 1993. Swimming of juvenile sea scallops, Placopecten magellanicus (Gmelin) - a minimum size for effective swimming. *J. Exp. Mar. Bio. Ecol.* **174**: 137–175.

Mason, G.E., Sameoto, J.A. & Metaxas, A. 2014. In situ swimming characteristics of the sea scallop, Placopecten magellanicus, on German Bank, Gulf of Maine. *J. Mar. Biol. Assoc. United Kingdom* **94**: 1019–1026.

Millward, A. & Whyte, M.A. 1992. The hydrodynamic characteristics of six scallops in the superfamily Pectinacea, Class Bivalvia. *J. Zool.* **227**: 547–566.

Mitteroecker, P. & Gunz, P. 2009. Advances in Geometric Morphometrics. *Evol. Biol.* **36**: 235–247.

Morton, B. 1980. Swimming in Amusium pleuronectes (Bivalvia: Pectinidae). *J. Zool.* **190**: 375–404.

Muschick, M., Indermauer, A. & Salzburger, W. 2012. Convergent evolution within an adaptive radiation of cichlid fish. *Curr. Biol.* **22**: 1–7.

Mynhardt, G., Alejandrino, A., Puslednik, L., Corrales, J. & Serb, J. 2015. Shell shape convergence masks biological diversity in gliding scallops: description of Ylistrum n.gen. (Pectinidae) from the Indo-Pacific Ocean. *J. Molluscan Stud.*

Pennel, M., Eastman, J., Slater, G., Brown, J., Uyeda, J., Fitzjohn, R., *et al.* 2014. geiger v2.0: an expanded suite of methods for fitting macroevolutionary models to phylogenetic trees. *Bioinformatics* **30**: 2216–2218.

Puslednik, L. & Serb, J.M. 2008. Molecular phylogenetics of the Pectinidae (Mollusca: Bivalvia) and the effect of outgroup selection and increased taxon sampling on tree topology. *Mol. Phylogenet. Evol.* **48**: 1178–1188.

R Core Team. 2017. R: a language and environment for statistical computing. RFoundation for Statistical Computing, Vienna.

Rambaut, A., Suchard, M., Xie, D. & Drummond, A. 2014. Tracer v1.6, available from http://beast.bio.ed.ac.uk/Tracer.

Rohlf, F.J. 1990. Morphometrics. *Annu. Rev. Ecol. Syst.* **21**: 299–316.

Rohlf, F.J. & Slice, D.E. 1990. Extensions of the Procrustes method for the optimal superimposition of landmarks. *Syst. Zool.* **39**: 40–59.

Serb, J. 2016. Reconciling morphological and molecular approaches to develop a phylogeny for the Pectinidae (Mollusca: Bivalvia). In: *Scallops: Biology, Ecology and Aquaculture* (G. J. Parsons & S. E. Shumway, eds), pp. 1–29. Elseiver.

Serb, J.M., Alejandrino, A., Otárola-Castillo, E. & Adams, D.C. 2011. Shell shape quantification using geometric morphometrics reveals morphological convergence of distantly related scallop species (Pectinidae). *Zool. J. Linn. Soc.* **163**: 571–584.

Sherratt, E., Alejandrino, A., Kraemer, A., Adams, D. & Serb, J. 2016. Trends in the sand: directional evolution in the shell shape of recessing scallops (Bivalvia: Pectinidae). *Evolution (N. Y).* **70**: 2061–2073.

Sidlauskas, B. 2008. Continuous and arrested morphological diversification in sister clades of characiform fishes: A phylomorphospace approach. *Evolution (N. Y).* **62**: 3135–3156.

Smith, E. 1902. Report on the collections of natural history made in the Antarctic region during the voyage of the "Southern Cross." In: *Mollusca* (I. Franklin, ed), pp. 201–213.

Stanley, S.M. 1972. Functional morphology and evolution of bysally attached bivalve mollusks. *J. Paleontol.* **46**: 165–212.

Stanley, S.M. 1970. Relation of shell form to life habits of the Bivalvia (Mollusca). *Geol. Soc. Am. Mem.* **125**: 1–296.

Stayton, C.T. 2014. convevol: Quantifies and assesses the significance of convergent evolution. R package version 1.0. Available at http://cran.r-project.org/web/packages/convevol/index.html.

Stayton, C.T. 2008. Is convergence surprising? An examination of the frequency of convergence in simulated data sets. *J. Theor. Biol.* **252**: 1–14.

Stayton, C.T. 2006. Testing hypotheses of convergence with multivariate data: morphological and functional convergence among herbivorous lizards. *Evolution (N. Y).* **60**: 824–841.

Stayton, C.T. 2015. The definition, recognition, and interpretation of convergent evolution, and two new measures for quantifying and assessing the significance of convergence. *Evolution (N. Y).* **69**: 2140–2153.

Talavera, G. & Castresana, J. 2007. Improvement of phylogenies after removing divergent and ambiguously aligned blocks from protein sequence alignments. *Syst. Biol.* **56**: 564–77.

Thomas, R.D.K. 1978. Shell form and the ecological range of living and extinct Arcoida. *Paleobiology* **4**: 181–194.

Thompson, J.D., Higgins, D.G. & Gibson, T.J. 1994. CLUSTAL W: improving the sensitivity of progressive multiple sequence alignment through sequence weighting, position-specific gap penalties and weight matrix choice. *Nucleic Acids Res.* **22**: 4673–4680.

Tremblay, I., Samson-Dô, M. & Guderley, H.E. 2015. When behavior and mechanics meet: scallop swimming capacities and their hinge ligament. *J. Shellfish Res.* **34**: 203–212.

Verrill, A.E. 1897. A study of the family Pectinidae, with a revison of genera and subgenera. *Trans. Connect. Acad. Arts Sci.* **10**: 41–95.

Vincent, S.E., Brandley, M.C., Herrel, A. & Alfaro, M.E. 2009. Convergence in trophic morphology and feeding performance among piscivorous natricine snakes. *J. Evol. Biol.* **22**: 1203–1211.

Wainwright, P.C. 2007. Functional Versus Morphological Diversity in Macroevolution. *Annu.*

Rev. Ecol. Evol. Syst. **38**: 381–401.

Wainwright, P.C., Alfaro, M.E., Bolnick, D.I. & Hulsey, C.D. 2005. Many-to-one mapping of form to function: A general principle in organismal design? *Integr. Comp. Biol.* **45**: 256–262.

Williams EE. 1972. The origin of faunas. Evolution of lizard congeners in a complex island fauna: A trial analysis. *Evol. Biol.* **6**: 47–89.

Wroe, S. & Milne, N. 2007. Convergence and remarkably consistent constraint in the evolution of carnivore skull shape. *Evolution (N. Y).* **61**: 1251–1260.

Zelditch, M.L., Swiderski, D.L. & Sheets, H.D. 2012. *Geometric Morphometrics for Biologists: A Primer*, 2nd ed. Academic Press.

Zelditch, M.L., Ye, J., Mitchell, J.S. & Swiderski, D.L. 2017. Rare ecomorphological convergence on a complex adaptive landscape: body size and diet mediate evolution of jaw shape in squirrels (Sciuridae). *Evolution (N. Y).*, doi: 10.1111/evo.13168.

Tables

Table 1 Levels of morphological disparity (MD) among species within each ecomorph. The first row represents MD obtained using standard approaches while the second row contains measures obtained while accounting for phylogenetic non-independence among taxa. MD for the nestling ecomorph is not shown, as there was only one species represented in this study.

Ecomorph	Byssal attaching	Cementing	Free-living	Gliding	Recessing
MD: Standard	2.144×10^{-3}	2.079×10^{-3}	3.593×10^{-3}	1.937×10^{-3}	2.036×10^{-3}
MD: Phylogenetic	6.515×10^{-5}	3.949×10^{-5}	1.055×10^{-4}	3.286×10^{-5}	1.186×10^{-4}

Table 2 Some aspects of swimming performance during the horizontal phase in gliding scallops from the A and B morphotypes (indicated in parentheses).

	A. pleuronectes (A)*	*Y. balloti* (A) †	*P. magellanicus* (B)‡	*Ad. colbecki* (B) ¶
Distance traveled (m)	1-10 N/A	1.0-23.1 mean = 8.01 ± 4.57 (n = 200)	0.26-3.26 mean = 1.44 ± 0.599 (n = 126)	0.11-2.03 mean = 0.276 ± 0.14 (n = 9)
Number of adductions	10-50 mean = 22.968 ± 9.816 (n = 29)	N/A	8-21§ mean = 13.38 ± 3.49 (n = 32)	1-18 mean = 2.44 ± 1.24 (n = 9)
Swimming time (s)	5-18 mean = 9.72 ± 3.1327 (n = 32)	N/A	1.2-7.4 mean = 3.1 ± 1.2 (n = 126)	0.86-10.16 mean = 1.72 ± 0.78 (n = 9)
Swimming velocity (m/s)	0.23-0.73 mean = 0.39 ± 0.107 (n = 37)	0.2-1.6 mean = 0.86 ± 0.288 (n = 25)	0.42-1.03 mean = 0.474 ± 0.166 (n = 200)	0.19-0.43 mean = 0.157 ± 0.04 (n = 7)

* Morton, 1980
† Joll, 1989
‡ Mason *et al.* 2014
§ Caddy, 1968
¶Ansell, 1998

Table 3 Results from pairwise t-tests (T) comparing performance measures between members of the A morphotype and the B morphotype. All comparisons were statistically significant at the experiment-wise Bonferroni value ($P < 0.005$) unless indicated.

	Distance traveled		Number of adductions		Swimming time		Swimming velocity	
	T	*P*	T	*P*	T	*P*	T	*P*
Y_balloti (A) vs. *P_magellanicus* (B)	39.54	2.46×10^{-126}	N/A		N/A		3.47	3.08×10^{-4}
Y_balloti (A) vs. *Ad_colbecki* (B)	39.46	1.41×10^{-98}	N/A		N/A		5.35	4.27×10^{-6}
A_pleuronectes (A) vs. *P_magellanicus* (B)	N/A		16.07	1.27×10^{-39}	20.19	1.09×10^{-45}	0.47	0.316 NS
A_pleuronectes (A) vs. *Ad_colbecki* (B)	N/A		29.20	3.06×10^{-27}	18.60	2.61×10^{-21}	1.23	0.112 NS

Figure legends

Figure 1 Three-dimensional surface scan of the left valve of a scallop with the position of landmarks and semilandmarks indicated as silver spheres. Five landmarks are numbered and represented by large spheres: Landmark 1 ventroposterior auricle; Landmark 2 dorsoposterior auricle; Landmark 3 umbo; Landmark 4 dorsoanterior auricle; Landmark 5 ventroanterior auricle. Semilandmarks are shown as small spheres. Redrawn from Sherratt *et al*. (2016).

Figure 2 Pruned chronogram of 93 scallop species for which morphological data is available. Species labels are colored by life habit (green = cementing, red = nestling, blue = byssal attaching, purple = recessing, black = free-living, orange = gliding). Left valves of the six gliding species are shown on the right (marked by letters a-f). Genera and species as in Table S2. Time calibration based upon 30 node groups. Redrawn from Sherratt *et al*. (2016).

Figure 3 Principal components plot of shell shape based on 933 specimens. The first two axes explain 66.7% of the total shape variation (PC1 = 42%; PC2 = 24.6%). Specimens are colored by the life habit group to which they belong (legend inset, ordered by increasing mobility). Shape deformations relating to the positive and negative extremes of each axis are shown as surfaces warped using thin-plate spline, depicted in dorsal (left) and lateral (right) views.

Figure 4 Phylomorphospace plot visualizing the first two axes of morphospace of scallops, with the phylogeny superimposed for 93 species. Colored dots represent extant species and white dots represent hypothesized ancestors inferred from ancestral state reconstruction. The inset shows an enlargement of the region in morphospace containing gliding species with orange dots,

displaying the two gliding morphotypes (A and B). Only those phylogenetic branches containing gliding species and their ancestors (squares) are shown.

Supporting information

Additional Supporting Information may be found online in the supporting information tab for this article:

Fig. S1 Chronogram of 143 scallop species.

Fig. S2 Axes 2 and 3 of a principal components plot of shell shape based on 933 specimens, plotted as PC3 *vs* 2 to be compared side-by-side with Figure 3. Together, PCs 1-3 explain 78.8% of the variation (PC2 = 24.6%, PC3 = 12.2%; subsequent axes each contribute less than 5% of the total shape variation). Specimens are colored by the life habit group to which they belong (legend inset, ordered by increasing mobility). Shape deformations relating to the positive and negative extremes of PC3 are shown as surfaces warped using thin-plate spline, depicted in dorsal (left) and lateral (right) views.

Table S1 Scallop behavioral life habit categories for morphological specimens.

Table S2 Genbank accession numbers for 143 specimens included in the molecular phylogeny.

Data deposited at Dryad (need to update): doi:10.5061/dryad.43548.

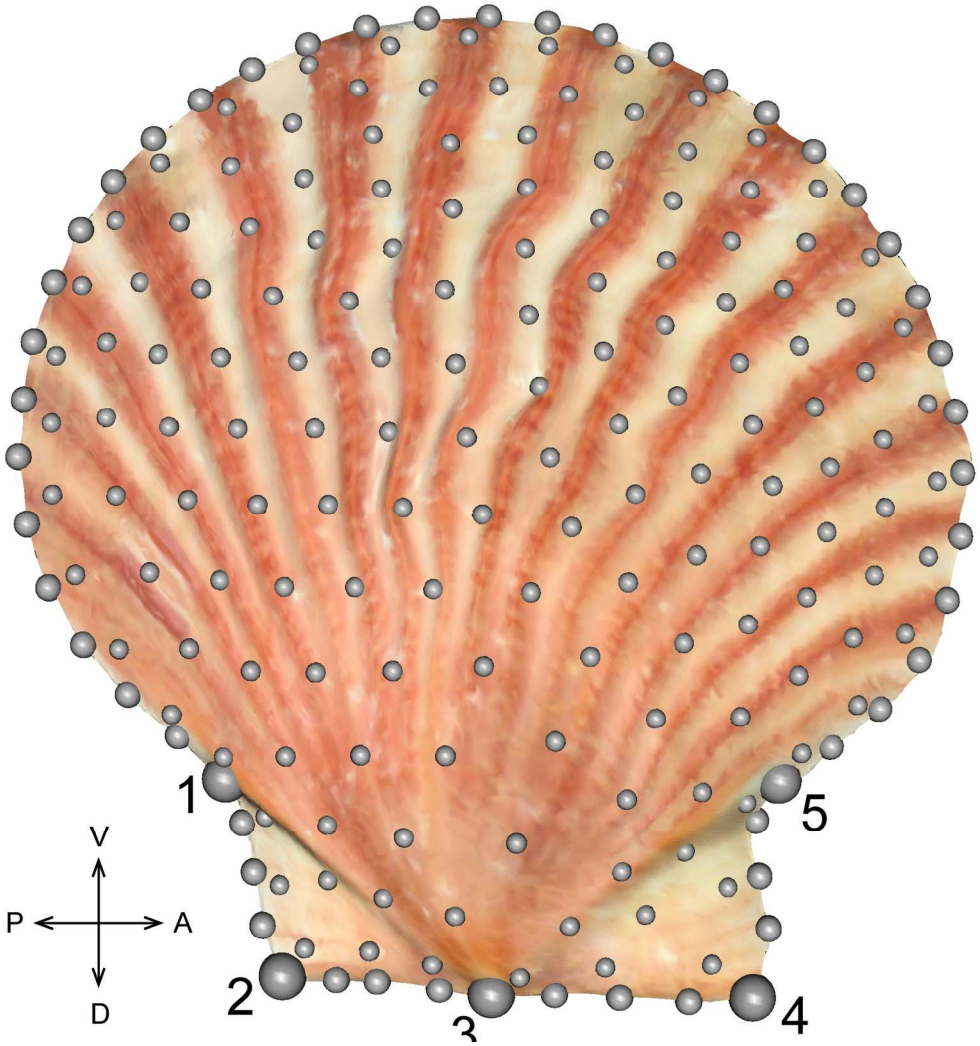

Three-dimensional surface scan of the left valve of a scallop, with the position of landmarks and semilandmarks indicated as silver spheres. Five landmarks are numbered and represented by large spheres and the semilandmarks are shown as small spheres. Landmark 1: ventroposterior auricle, 2: dorsoposterior auricle, 3: umbo, 4: dorsoanterior auricle, 5: ventroanterior auricle.

171x181mm (300 x 300 DPI)

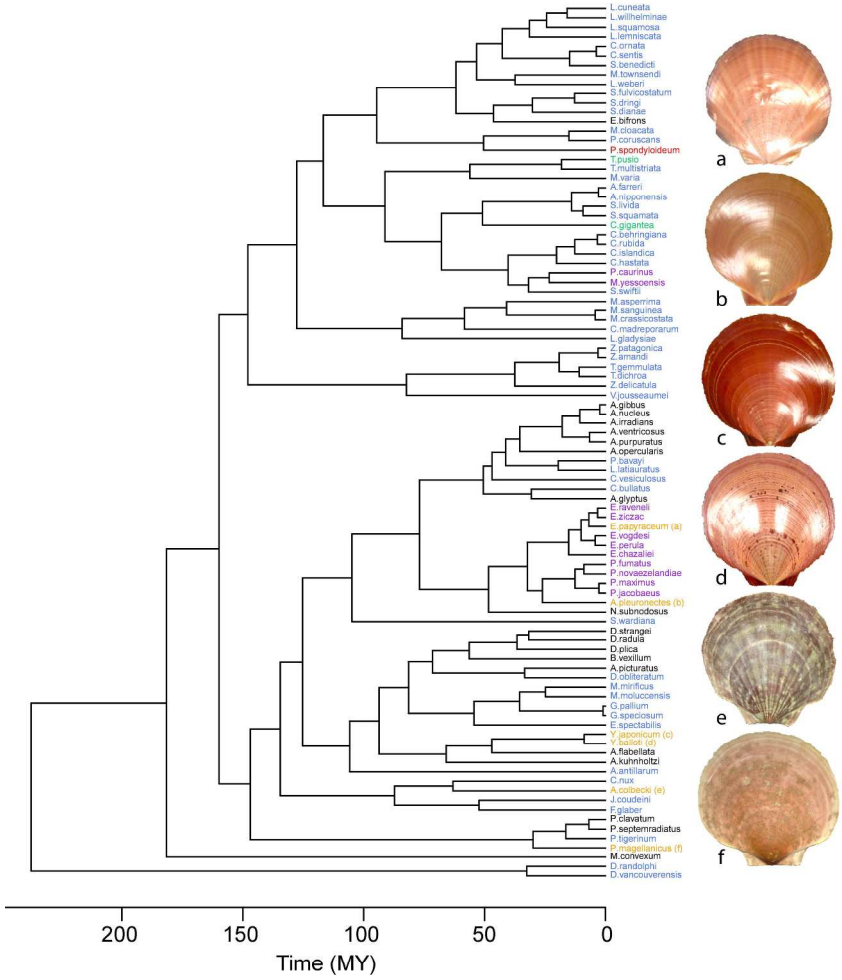

Pruned chronogram of 93 scallop species with morphological data. Species labels are colored by life habit (green = cementing, red = nestling, blue = byssal attaching, purple = recessing, black = free-living, orange = gliding). Left valves of the six gliding species are shown on the right (marked by letters a-f). Genera and species as in Table S2. Time calibration based upon 30 node groups.

234x307mm (300 x 300 DPI)

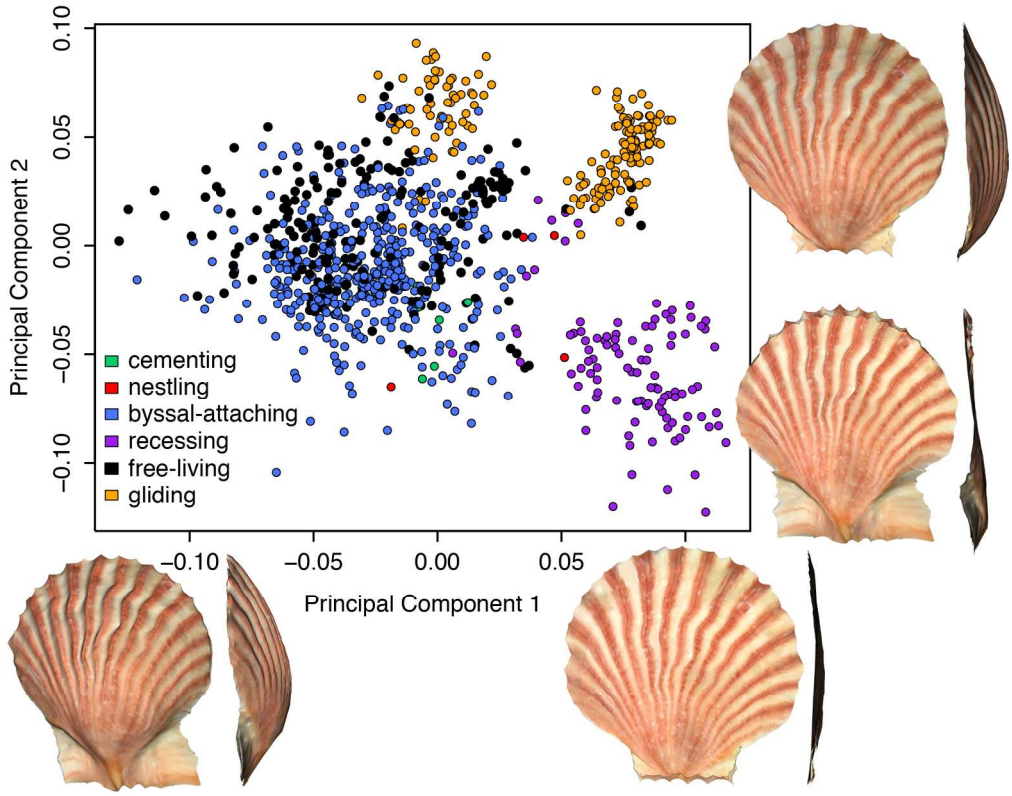

Figure 3 Principal components plot of shell shape based on 933 specimens. The first two axes explain 66.7% of the total shape variation (PC1 = 42%; PC2 = 24.6%). Specimens are colored by the ecomorph to which they belong (legend inset, ordered by increasing mobility). Shape deformations relating to the positive and negative extremes of each axis are shown as surfaces warped using thin-plate spline, depicted in dorsal (left) and lateral (right) views.

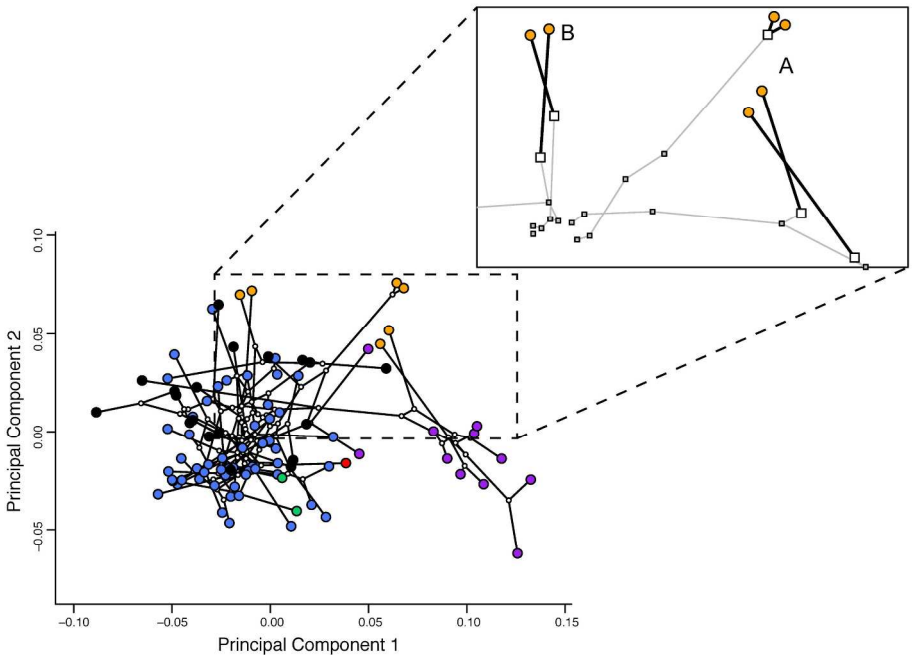

Phylomorphospace plot visualizing the first two axes of morphospace of scallops, with the phylogeny superimposed. Colored dots represent extant species and white dots represent hypothesized ancestors found from ancestral state reconstruction. The inset shows an enlargement of the region in morphospace containing gliding species with orange dots, displaying the two gliding morphotypes (A and B). Only those phylogenetic branches containing gliding species and their ancestors (squares) are shown.

234x307mm (300 x 300 DPI)

Supporting Information for

Phylogenetic convergence and multiple shell shape optima for gliding scallops (Bivalvia: Pectinidae)

(2 supplementary figures and 2 supplementary tables)

Figure S1 Chronogram of 143 scallop species**.** A time-calibrated phylogeny constructed from all molecular data available. Species in grey are those not included in this morphological study, including five outgroups. Remaining 93 species for which we had morphometric data are colored by life habit (green = cement, red = nestle, blue = byssal, purple = recess, black = free, orange = glide). Red dots indicate the fossil calibration points (details in Table 2). Blue bars represent 95% CI.

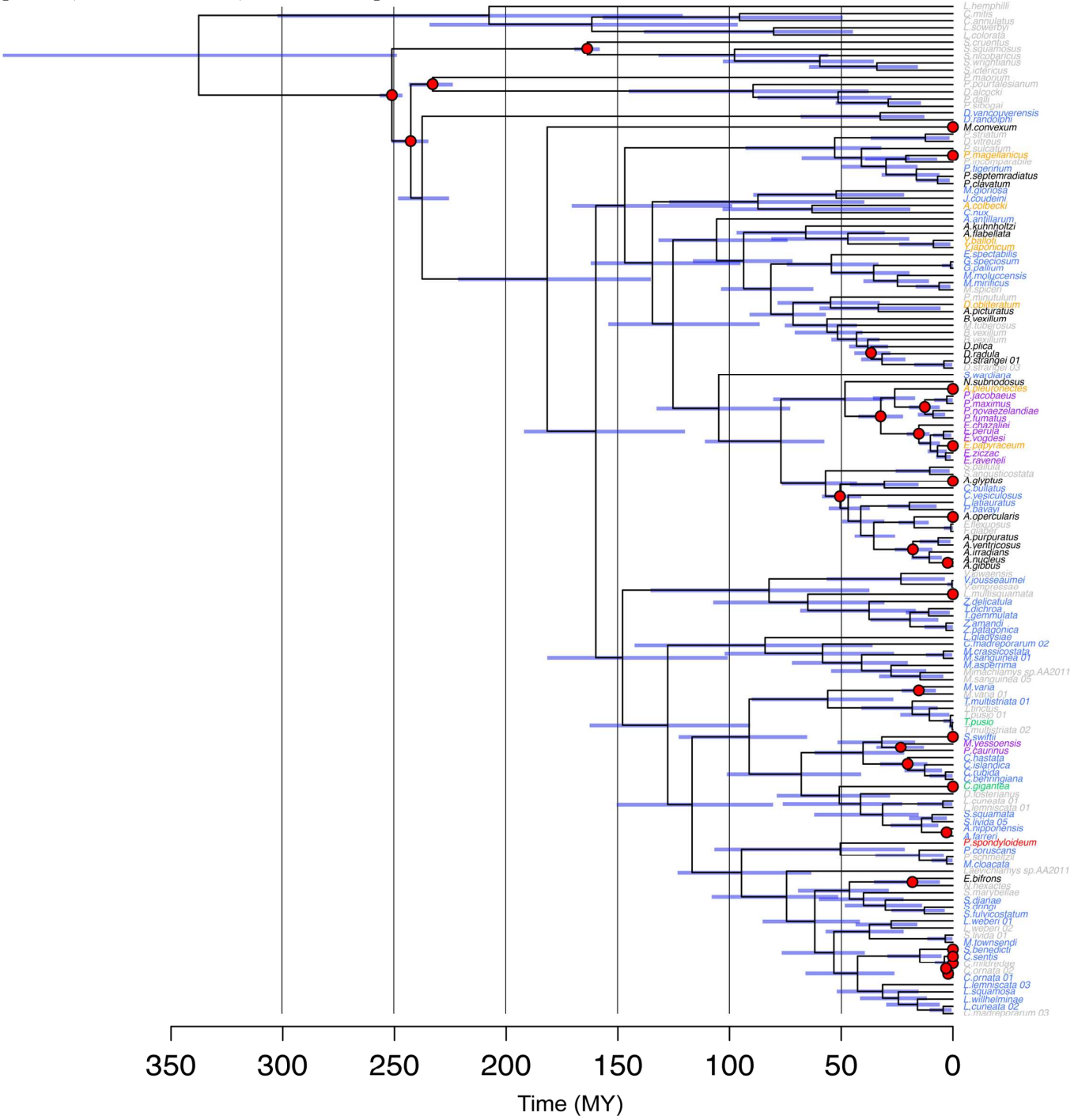

Figure S2 Axes 2 and 3 of a principal components plot of shell shape based on 933 specimens, plotted as PC3 *vs* 2 to be compared side-by-side with Figure 3. Together, PCs 1-3 explain 78.8% of the variation (PC2 = 24.6%, PC3 = 12.2%; subsequent axes each contribute less than 5% of the total shape variation). Specimens are colored by the life habit group to which they belong (legend inset, ordered by increasing mobility). Shape deformations relating to the positive and negative extremes of PC3 are shown as surfaces warped using thin-plate spline, depicted in dorsal (left) and lateral (right) views.

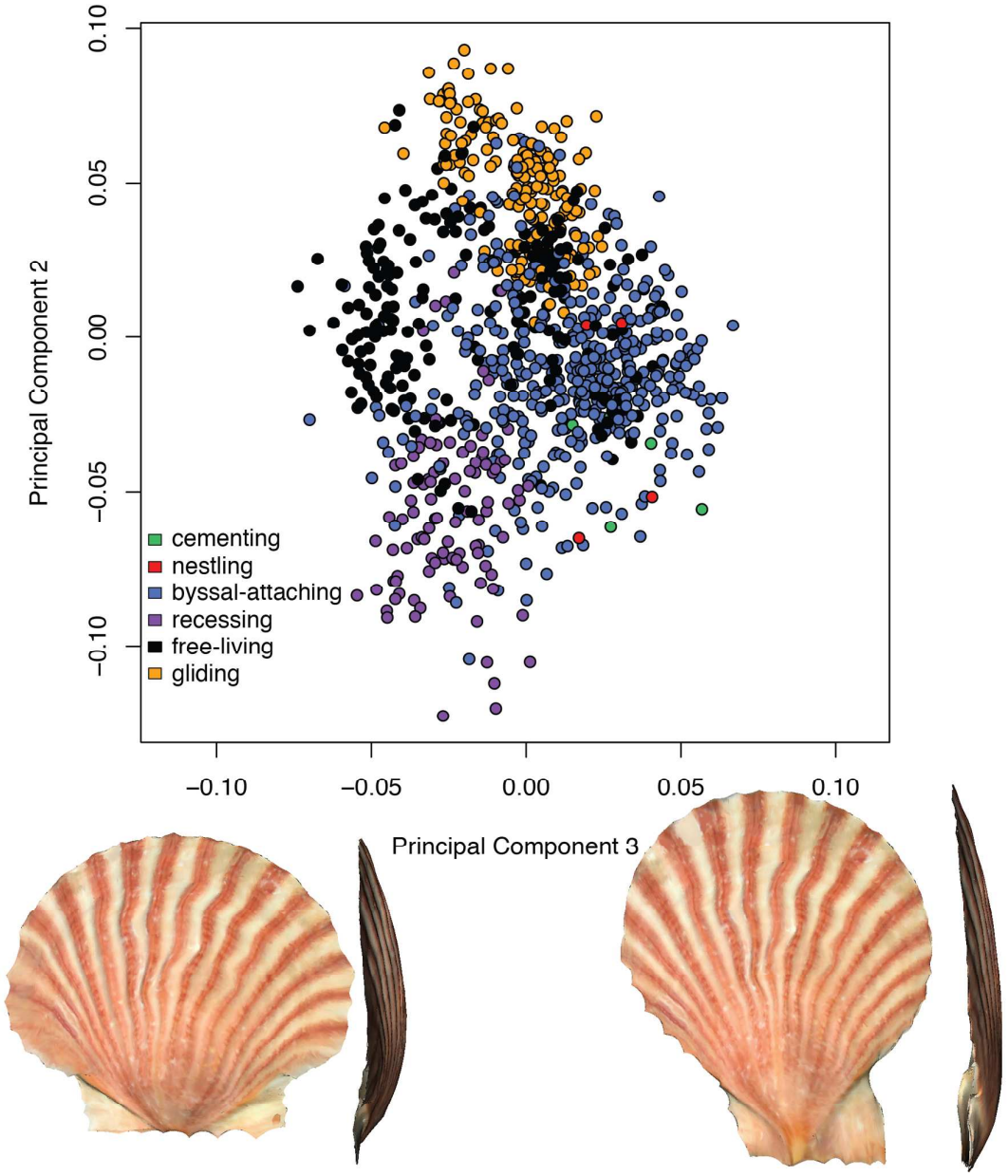

Table S1 Scallop behavioral life habit categories for morphological specimens. The phylogeny ID corresponds to the tip label of Figure 2 (and Figure S1). Number of specimens used (No. spec.) to calculate the average for each species were taken from museum collections, summarized here using the official museum acronyms.

Species	Phylogeny ID	Habit	No. spec.	Museum
Adamussium colbecki	A.colbecki	glide	39	USNM
Aequipecten glyptus	A.glyptus	free	5	FMNH
Aequipecten opercularis	A.opercularis	free	7	FMNH
Amusium pleuronectes	A.pleuronectes	glide	30	USNM
Anguipecten picturatus	A.picturatus	free	3	MNHN
Annachlamys flabellata	A.flabellata	free	5	UF
Annachlamys kuhnholtzi	A.kuhnholtzi	free	2	MNHN
Antillipecten antillarum	A.antillarum	byssal	7	UF; LACM; USNM; LACM
Argopecten gibbus	A.gibbus	free	5	LACM
Argopecten irradians	A.irradians	free	28	DMNH
Argopecten nucleus	A.nucleus	free	10	LACM
Argopecten purpuratus	A.purpuratus	free	25	UF
Argopecten ventricosus	A.ventricosus	free	6	LACM; CAS
Azumapecten farreri	A.farreri	byssal	5	LACM; BPBM
Azumapecten nipponensis	A.nipponensis	byssal	2	AMNH
Bractechlamys vexillum	B.vexillum	free	10	LACM
Caribachlamys ornata	C.ornata	byssal	2	BPBM
Caribachlamys sentis	C.sentis	byssal	30	UF
Chlamys behringiana	C.behringiana	byssal	19	
Chlamys hastata	C.hastata	byssal	13	MCZ; BPBM
Chlamys islandica	C.islandica	byssal	8	YPM; LACM
Chlamys rubida	C.rubida	byssal	5	BPBM
Coralichlamys madreporarum	C.madreporarum	byssal	9	LACM; MNHN
Crassadoma gigantea	C.gigantea	cement	1	NCSM
Cryptopecten bullatus	C.bullatus	byssal	2	MCZ; UF
Cryptopecten nux	C.nux	byssal	8	MNHN
Cryptopecten vesiculosus	C.vesiculosus	byssal	5	LACM
Decatopecten plica	D.plica	free	10	LACM
Decatopecten radula	D.radula	free	10	LACM; BPBM
Decatopecten strangei	D.strangei	free	6	LACM
Delectopecten randolphi	D.randolphi	byssal	3	MCZ
Delectopecten vancouverensis	D.vancouverensis	byssal	7	LACM
Dentamussium obliteratum	D.obliteratum	glide	5	LACM; DMNH
Equichlamys bifrons	E.bifrons	free	9	LACM; DMNH; BPBM
Euvola chazaliei	E.chazaliei	recess	5	NCSM; AMNH
Euvola papyraceum	E.papyraceum	glide	14	FMNH
Euvola perula	E.perula	recess	7	UF
Euvola raveneli	E.raveneli	recess	7	LACM; YPM
Euvola vogdesi	E.vogdesi	recess	12	LACM; USNM
Euvola ziczac	E.ziczac	recess	28	FMNH; LACM
Excellichlamys spectabilis	E.spectabilis	byssal	16	LACM
Flexopecten glaber	F.glaber	byssal	2	MNHN; YPM
Gloripallium pallium	G.pallium	byssal	9	FMNH

Gloripallium speciosum	G.speciosum	byssal	8	LACM
Juxtamusium coudeini	J.coudeini	byssal	6	MNHN
Laevichlamys gladysiae	L.gladysiae	byssal	5	MNHN
Laevichlamys cuneata	L.cuneata	byssal	8	LACM; MNHN
Laevichlamys lemniscata	L.lemniscata	byssal	5	LCSM; MCZ; DMNH
Laevichlamys squamosa	L.squamosa	byssal	8	MNHN; CAS
Laevichlamys weberi	L.weberi	byssal	5	CAS; USNM
Laevichlamys willhelminae	L.willhelminae	byssal	4	USNM
Leptopecten latiauratus	L.latiauratus	byssal	5	BPBM; NCSM; CAS
Mesopeplum convexum	M.convexum	free	5	MCZ; DMNH
Mimachlamys asperrima	M.asperrima	byssal	7	LACM
Mimachlamys cloacata	M.cloacata	byssal	7	MNHN; USNM
Mimachlamys crassicostata	M.crassicostata	byssal	10	FMNH
Mimachlamys sanguinea	M.sanguinea	byssal	5	MCZ; USNM; CAS
Mimachlamys townsendi	M.townsendi	byssal	5	USNM; AMNH
Mimachlamys varia	M.varia	byssal	8	FLMNH
Mirapecten mirificus	M.mirificus	byssal	4	BPBM; DMNH
Mirapecten moluccensis	M.moluccensis	byssal	1	MNHN
Mizuhopecten yessoensis	M.yessoensis	recess	5	CAS; UF; AMNH
Nodipecten subnodosus	N.subnodosus	free	4	LACM; YPM
Palliolum tigerinum	P.tigerinum	byssal	2	CAS
Paraleptopecten bavayi	P.bavayi	byssal	5	DAMNH; UF
Pascahinnites coruscans	P.coruscans	byssal	8	FMNH USNM
Patinopecten caurinus	P.caurinus	recess	4	CAS, MCZ; DMNH
Pecten fumatus	P.fumatus	recess	17	LACM
Pecten jacobaeus	P.jacobaeus	recess	5	NCSM; YPM
Pecten maximus	P.maximus	recess	6	LACM
Pecten novaezelandiae	P.novaezelandiae	recess	5	NCSM
Pedum spondyloideum	P.spondyloideum	nestle	4	MNHN; USNM;YPM
Placopecten magellanicus	P.magellanicus	glide	24	
Pseudamussium clavatum	P.clavatum	free	5	MCZ; AMNH
Pseudamussium septemradiatus	P.septemradiatus	free	28	USNM
Scaeochlamys livida	S.livida	byssal	5	FMNH; YPM; BPBM
Scaeochlamys squamata	S.squamata	byssal	5	MNHN; USNM
Semipallium dianae	S.dianae	byssal	3	MCZ; DMNH
Semipallium dringi	S.dringi	byssal	24	MCZ; MNHN
Semipallium fulvicostatum	S.fulvicostatum	byssal	5	MNHN; YPM; BPBM
Semipallium wardiana	S.wardiana	byssal	1	AMNH
Spathochlamys benedicti	S.benedicti	byssal	5	FMNH; DMNH
Swiftopecten swiftii	S.swiftii	byssal	8	DMNH; CAS
Talochlamys dichroa	T.dichroa	byssal	3	MNHN; DMNH
Talochlamys gemmulata	T.gemmulata	byssal	5	AMNH; BPBM; UF; MCZ
Talochlamys multistriata	T.multistriata	byssal	4	MNHN
Talochlamys pusio	T.pusio	cement	5	BPBM; YPM; DMNH?
Veprichlamys jousseaumei	V.jousseaumei	byssal	5	MCZ
Ylistrum balloti	Y.balloti	glide	39	WAMS; BALD ISL
Ylistrum japonicum	Y.japonicum	glide	36	LACM; USNM
Zygochlamys amandi	Z.amandi	byssal	3	USNM

Zygochlamys delicatula	Z.delicatula	byssal	5	AMNH; MCZ
Zygochlamys patagonica	Z.patagonica	byssal	14	BPBM; YPM; LACM; UF

Table S2 Genbank accession numbers for 143 specimens included in the molecular phylogeny. Outgroup species indicated by asterisk (*). The phylogeny ID corresponds to the tip labels of Figure 2 and Figure S1. When available, morphological vouchers are listed by museum and collection accession number: AMNH = American Museum of Natural History; MNHN = Muséum National d'Histoire Naturelle, Paris, France; NIWA = National Institute Water and Atmospheric Research, New Zealand; QM = Queensland Museum, Australia; TM = Tepapa Museum, New Zealand; UF = Florida Museum of Natural History, Gainesville, Florida, United States; USC = University of the Sunshine Coast Pectinid Collection, Queensland, Australia; USNM = United States National Museum, Smithsonian Institution.

Species	Phylogeny ID	Locality	12S Genbank	16S Genbank	H3 Genbank	28S Genbank	Voucher
Adamussium colbecki	A.colbecki	Terra Nova Bay, Antarctica	EU379383	EU379437	EU379491	FJ263652	Serb lab
Aequipecten glyptus	A.glyptus	Gulf of Mexico, Florida, USA	EU379391	EU379445	EU379499	HM622699	UF351155
Aequipecten opercularis	A.opercularis	Millport, Scotland	EU379408	EU379462	EU379516	HM630527	Serb lab
Amusium pleuronectes	A.pleuronectes	Rayong Province, Thailand	EU379415	EU379469	EU379523	HM630508	USNM 1236642
Anguipecten picturatus	A.picturatus	Mariana Islands	HM630510	HM630511	HM630512	HM630513	UF288930
Annachlamys flabellata	A.flabellata	Yeppoon, QLD, Australia	KP300578	KP300544	KP300481	KP300515	USC SCALL151-153
Annachlamys kuhnholtzi	A.kuhnholtzi	Gladstone, QLD, Australia	KP300587	KP300553	KP300490	KP300522	USC SCALL151-155
Antillipecten antillarum	A.antillarum	unknown	HM535656	HM535657	HM535658	HM535659	
Argopecten gibbus	A.gibbus	Harrington Sound, Bermuda	EU379388	EU379442	EU379496	HM622697	Serb lab
Argopecten irradians	A.irradians	Gulf of Mexico, Florida, USA	EU379392	EU379446	EU379500	HM622700	Serb lab
Argopecten nucleus	A.nucleus	Key Largo, Florida, USA	EU379406	EU379460	EU379514	HM630528	AMNH 298075
Argopecten purpuratus	A.purpuratus	Tongoy Bay, Chila	EU379417	EU379471	EU379525	HM630495	N/A
Argopecten ventricosus	A.ventricosus	Bahia Magdalena, Baja California Sur, Mexico	HM630407	HM630408	HM630409	HM630410	Serb lab
Azumapecten f. farreri	A.farreri	Aquaculture Facility in Qindao, China	HM622677	HM622678	HM622679	HM622680	Serb lab
Azumapecten f. nipponensis	A.nipponensis	Kitaibaraki City, Japan	HM622685	HM622686	HM622687	HM622688	Serb lab
Bractechlamys vexillum	B.vexillum	West Great Palm Island, QLD, Australia	KP300601	KP300566	KP300504	N/A	QM SBD005517

Bractechlamys vexillum	B.vexillum	Cebu Island, Philippines	HM630395	HM630396	HM630397	HM630398	UF313444
Bractechlamys vexillum	B.vexillum	Phuket, Thailand	HM630391	HM630392	HM630393	HM630394	UF281663
Caribachlamys mildredae	C.mildredae	N of Crawl Cay, Bocase del Toro, Panama	HM630541	HM630542	HM630543	HM630544	UF289624
Caribachlamys ornata	C.ornata	La Parquera, Collao, Puerto Rico	HM630379	HM630380	HM630381	HM630382	Serb lab
Caribachlamys ornata	C.ornata02	La Parquera, Collao, Puerto Rico	HM630375	HM630376	HM630377	HM630378	Serb lab
Caribachlamys sentis	C.sentis	unknown	GU953232	GU953234	GU953233	HM630478	UF313459
Chlamys rubida	C.rubida	San Juan Island, Washington, USA	FJ263636	FJ263645	FJ263665	FJ263655	Serb lab
Chlamys behringiana	C.behringiana	Monti Bay, Yakutat, Alaska, USA	FJ263632	FJ263641	FJ263661	FJ263650	Serb lab
Chlamys hastata	C.hastata	San Juan Island, Washington, USA	FJ263639	FJ263648	FJ263667	FJ263658	Serb lab
Chlamys islandica	C.islandica	Quebec, Canada	FJ263637	FJ263646	FJ263666	FJ263656	Serb lab
Complichlamys wardiana	S.wardiana	Lady Musgrave Island, QLD, Australia	KP300602	KP300567	KP300505	KP300534	QM SBD026668
Coralichlamys madreporarum	C.madreporarum03	Viti Levu Island, Fiji	EU379396	EU379450	EU379504	HM630548	UF296052
Coralichlamys madreporarum	C.madreporarum	Sabben Island, Bismarck Archipelago, Papua New Guinea	EU379397	EU379451	EU379505	HM630547	UF323809
Crassadoma giganeta	C.gigantea	Santa Barbara, California, USA	FJ263635	FJ263644	FJ263664	FJ263654	Serb lab
Cryptopecten bullatus	C.bullatus	Bohol Sea, off Balicasag Island, Philippines	KP300573	KP300539	KP300476	KP300510	MNHN IM-2007-33796
Cryptopecten nux	C.nux	Low Wooded Island, QLD, Australia	KP300594	KP300560	KP300497	KP300527	QM SBD001138
Cryptopecten vesiculosus	C.vesiculosus	Miura City, Japan	HM630403	HM630404	HM630405	HM630406	Serb lab
Ctenoides annulatus*	C.annulatus	Bismark Archipelago, Papua New Guinea	EU379385	EU379439	EU379493	HM535655	UF322180
Ctenoides mitis*	C.mitis	Florida Keys, Long Point Park, USA	EU379386	EU379440	EU379494	HM600745	UF367478
Decatopecten plica	D.plica	Tateyama, Japan	HM630435	HM630436	HM630437	HM630438	Serb lab

Decatopecten radula	D.radula	Sulawsi Island, Indonesia	N/A	HM630492	HM630493	HM630494	UF280376
Decatopecten strangei	D.strangei01	Western Australia, Australia	HM630439	HM630440	HM630441	HM630442	UF296996
Decatopecten strangei	D.strangei03	Great Barrier Reef, QLD, Australia	KP300598	KP300564	KP300501	KP300531	QM SBD004329
Delectopecten fosterianus	D.fosterianus	Chatham Rise, New Zealand	KP300579	KP300545	KP300482	N/A	NIWA 29947
Delectopecten randolphi	D.randolphi	Hitachi City, Japan	HM630488	HM630489	HM630490	HM630491	Serb lab
Delectopecten vancouverensis	D.vancouverensis	North Pacific Ocean; 32°36'N; 117°30.5'W	HM630418	HM630420	HM630416	HM630417	Scripps Inst Oceanography
Delectopecten vitreus	D.vitreus	Skagerrak, Sweden	JQ611464	JQ611441	JQ611553	JQ611530	Genbank
Dentamussium obliteratum	D.obliteratum	E Aoré Island, Aimbuei Bay, Vanuatu	KP300595	KP300561	KP300498	KP300528	MNHN IM-2007-32426
Equichlamys bifrons	E.bifrons	Tasmania, Australia	HM561991	HM561992	HM561993	HM561994	Serb lab
Euvola chazaliei	E.chazaliei	Gulf of Los Mosquitos, Panama	EU379382	EU379436	EU379490	HM561999	Serb lab
Euvola papyraceum	E.papyraceum	Gulf of Mexico, USA	HM630371	HM630372	HM630373	HM630374	TCWC 40985
Euvola perula	E.perula	Pacific Ocean, Panama	EU379413	EU379467	EU379521	HM630515	Serb lab
Euvola raveneli	E.raveneli	Gulf of Mexico, Florida, USA	EU379419	EU379473	EU379527	HM630487	UF351301
Euvola vogdesi	E.vogdesi	Bahia Magdalena, Baja California Sur, Mexico	HM630387	HM630388	HM630389	HM630390	Serb lab
Euvola ziczac	E.ziczac	Harrington Sound, Bermuda	EU379430	EU379484	EU379538	HM630509	Serb lab
Execellichalmys spectabilis	E.spectabilis	Mariana Islands	HM630461	HM630462	HM630463	HM630464	UF282416
Flexopecten flexuosus	F.flexuosus	Alcocebre, Spain	JQ611465	JQ611442	JQ611554	JQ611531	Genbank
Flexopecten glaber	F.glaber	Rovinj, Croatia	JQ611466	JQ611443	JQ611569	JQ611532	Genbank
Gloripallium pallium	G.pallium	Viti Levu Island, Fiji	EU379410	EU379464	EU379518	HM630525	UF292105
Gloripallium speciosum	G.speciosum	Viti Levu Island, Fiji	HM630465	HM630466	HM630467	HM630468	UF292110
Juxtamusium coudeini	J.coudeini	Nymph Island, QLD, Australia	KP300575	KP300541	KP300478	KP300512	QM SBD005325
Laevichlamys cuneata (irregularis)	L.cuneata01	Tateyama City, Chiba, Japan	HM622702	HM622703	HM622704	HM622705	Serb lab
Laevichlamys cuneata	L.cuneata02	Milne Bay, Papua New	EU379429	EU379483	EU379537	HM622701	UF310406

(irregularis)		Guinea					
Laevichlamys cuneata (lemniscata)	L.lemniscata01	Tateyama City, Chiba, Japam	HM622715	HM622716	HM622717	HM622718	Serb lab
Laevichlamys lemniscata	L.lemniscata03	Port Ehoala, Madagascar	KP300588	KP300554	KP300491	KP300523	MNHN IM-2009-21008
Laevichlamys multisquamata	L.multisquamata	Pelican Point, St Maarten, Lesser Antilles	KP300593	KP300559	KP300496	N/A	UF348863
Laevichlamys sp.	Laevichlamys sp.AA2011	Japan	HM630469	HM630470	HM630471	HM630472	Serb lab
Laevichlamys wilhelminae	L.willhelminae	Great Barrier Reef, QLD, Australia	KP300605	KP300570	N/A	N/A	QM SBD036419
Laevichlamys gladysiae	L.gladysiae	16°04'N; 121°57'E, Philippines	KP300582	KP300548	KP300485	KP300518	MNHN IM-2007-33785
Laevichlamys weberi	L.weberi01	Phare Flacourt, Madagascar	KP300603	KP300568	KP300506	KP300535	MNHN IM-2009-21007
Laevichlamys weberi	L.weberi02	Cap Sainte Marie, Madagascar	KP300604	KP300569	KP300507	KP300536	MNHN IM-2009-20966
Leptopecten latiauratus	L.latiauratus	Goleta, California, USA	EU379393	EU379447	EU379501	HM622714	Serb lab
Levichlamys squamosa	L.squamosa	Okinawa, Japan	EU379426	EU379480	EU379534	HM630443	UF351954
Lima coloratazealandica*	L.colorata	North Cape, New Zealand	HM600760	HM600753	HM600733	HM600746	UF332786
Lima sowerbyi*	L.sowerbyi	Masirah Island, Oman	HM600763	HM600756	HM600736	HM600749	UF286387
Limaria hemphilli*	L.hemphilli		KP300584	KP300550	KP300487	N/A	
Mesopeplum convexum	M.convexum	Stewart Island, New Zealand	KP300574	KP300540	KP300477	KP300511	TM M297699
Mimachalmys cloacata	M.cloacata	Shiangjianwan, Taiwan	HM562000	HM562001	HM562002	HM562003	UF309990
Mimachalmys sanguinea	M.sanguinea05	S of Faux Cap, Madagascar	KP300597	KP300563	KP300500	KP300530	MNHN IM-2009-20994
Mimachalmys sanguinea	M.sanguinea01	Thailand	HM630479	HM630480	HM630481	HM630482	Serb lab
Mimachalmys sp.	Mimachlamys sp.AA2011	Zanzibar Island, Tanzania	HM630473	HM630474	HM630475	HM630476	UF297000

Mimachalmys asperrima	M.asperrima	Hobart, Australia	HM540080	HM540081	HM540082	HM540083	Serb lab
Mimachlamys crassicostata	M.crassicostata	Kumatoto, Japan	HM630531	HM630532	HM630533	HM630534	Serb lab
Mimachlamys townsendi	M.townsendi	Masirah Island, Oman	HM630422	HM630423	HM630424	HM630425	UF292821
Mimachlamys gloriosa	M.gloriosa	E of Great Palm Island, QLD, Australia	KP300583	KP300549	KP300486	KP300519	QM SBD004187
Mimachlamys varia	M.varia	Rovinj, Croatia	JQ611468	JQ611446	JQ611557	JQ611535	Genbank
Mimachlamys varia	M.varia01	Gallicia, Spain	EU379428	EU379482	EU379536	HM630415	Serb lab
Mirapecten mirificus	M.mirificus	Saipan Island, Northern Mariana Islands	EU379401	EU379455	EU379509	HM630540	UF295809
Mirapecten spiceri	M.spiceri	Mariana Islands	EU379422	EU379476	EU379530	HM630456	UF282407
Mirapecten tuberosus	M.tuberosus	S of Faux Cap, Madagascar	KP300600	N/A	KP300503	KP300533	MNHN IM-2009-21009
Mirapecten moluccensis	M.moluccensis	Panglao Island, Bingag, Philippines	KP300592	KP300558	KP300495	KP300526	MNHN IM-2007-32456
Mizuhopecten yessoensis	M.yessoensis	Mutsu Bay, Japan	HM630383	HM630384	HM630385	HM630386	Serb lab
Nodipecten subnodosus	N.subnodosus	Pacific Ocean, Panama	EU379427	EU379481	EU379535	HM630434	Serb lab
Notochlamys hexates	N.hexactes	Edithburg, SA, Australia	KP300585	KP300551	KP300488	KP300520	USC SCALL201
Palliolum incomparabile	P.incomparabile	Skagerrak, Sweden	JQ611472	JQ611450	JQ611560	JQ611539	Genbank
Palliolum minutulum	P.mintulum	Aoré Island, Aimbuei Bay, Vanuatu	KP300591	KP300557	KP300494	KP300525	MNHN IM-2007-33927
Palliolum striatum	P.striatum	Skagerrak, Sweden	JQ611474	JQ611452	JQ611561	JQ611541	Genbank
Palliolum tigerinum	P.tigerinum	North Sea	JQ611475	JQ611453	JQ611562	JQ611542	Genbank
Paraleptopecten bavayi	P.bavayi	E of Naos, Panama	EU379381	EU379435	EU379487	HM540102	UF371875
Parvamussium maorium*	P.maorium	UTM -42.7871700, -176.7222000, New Zealand	KP300590	KP300556	KP300493	N/A	NIWA 22965
Patinopecten caurinus	P.caurinus	Yakutat Bay, Alaska, USA	FJ263633	FJ26642	FJ263662	FJ263651	Serb lab
Pecten fumatus	P.fumatus	Hobart, Tasmania, Australia	HM622689	HM622690	HM622691	HM622692	Serb lab
Pecten jacobaeus	P.jacobaeus	Bergen, Norway	JQ611477	JQ611455	JQ611564	JQ611544	Genbank
Pecten maximus	P.maximus	Millport, Scotland	EU379400	EU379454	EU379508	HM630545	
Pecten novaezelandiae	P.novaezelandiae	Mercury Cove, Great	EU379404	EU379458	EU379512	HM630530	Serb lab

		Mercury Island, New Zealand					
Pedum spondyloideum	P.spondyloideum	Stingray Shoals, Mariana Islands	HM630452	HM630453	HM630454	HM630455	UF343587
Placopecten magellanicus	P.magellanicus	Georges Bank, USA	FJ263638	FJ263647	EU379506	FJ263657	Serb lab
Propeamussium alcocki*	P.alcocki	14°50'N; 123°12'E, Philippines	KP300572	KP300537	KP300474	N/A	MNHN IM-2007-33735
Propeamussium dalli*	S.squamata	Dry Tortugas, Florida, USA	EU379416	EU379470	EU379524	HM600740	UF289879
Propeamussium pourtalesianum*	P.pourtalesianum	Florida Straits, Florida, USA	EU379411	EU379465	EU379519	HM600741	UF323764
Propeamussium sibogai	P.sibogai	NW of Nomamishaki, Kasasa-cho, Japan	HM600762	HM600755	HM600735	HM600748	Serb lab
Pseudamussium clavatum	P.clavatum	Portimao, Portugal	JQ611479	JQ611457	JQ611565	JQ611546	Genbank
Pseudamussium septemradiatus	P.septemradiatus	Millport, Scotland	EU379420	EU379474	EU379528	FJ263659	Serb lab
Pseudamussium sulcatum	P.sulcatum	Bergen, Norway	JQ611481	JQ611459	JQ611566	JQ611548	Genbank
Scaeochlamys livida	S.livida05	Masthead Island, QLD, Australia	KP300589	KP300555	KP300492	KP300524	QM SBD020910
Scaeochlamys livida	S.livida01	Muscat, Qurm, Oman	HM630549	HM630550	HM630551	HM630552	UF367882
Scaeochlamys squamata	S.squamata	Tateyama City, Chiba, Japan	HM630444	HM630445	HM630446	HM630447	Serb lab
Semipallium c. coruscans	P.coruscans	Cocos-Keeling Island, Australia	EU379384	EU379438	EU379492	HM600739	UF296350
Semipallium dianae	S.dianae	Ie Island, Okinawa, Japan	HM630553	HM630554	HM630555	HM630556	UF352388
Semipallium dringi	S.dringi	Ie Island, Okinawa, Japan	EU379387	EU379441	EU379495	HM622672	UF352373
Semipallium fulvicostatum	S.fulvicostatum	Lloyd Island, QLD, Australia	KP300580	KP300546	KP300483	KP300516	QM SBD020910
Semipallium marybellae	S.marybellae	Luminao Reef, Mariana Island, Guam	EU379399	EU379453	EU379507	HM630546	UF287521
Semipallium schmeltzii	P.schmeltzii	Maruki hama, Bonotsu City, Japan	HM630483	HM630484	HM630485	HM630486	Serb lab
Serratovola angusticostata	S.angusticostata	Dipolog Bay, Philippines	N/A	KP300538	KP300475	KP300509	MNHN IM-2007-33795

Serratovola pallula	S.pallula	E of Port Douglas, QLD, Australia	KP300596	KP300562	KP300499	KP300529	QM SBD000145
Spathochlamys benedicti	S.benedicti	W of Cedar Key, Florida, USA	HM540103	HM540104	HM540105	HM540106	UF369432
Spondylus cruentus*	S.cruentus	Tateyama City, Japan	HM600761	HM600754	HM600734	HM600747	Serb lab
Spondylus ictericus*	S.ictericus	Florida Keys, Florida, USA	EU379423	EU379477	EU379531	HM600742	UF367487
Spondylus squamosus*	S.squamosus	Shefa Province, Vanuatu	EU379425	EU379479	EU379533	HM600744	UF368676
Spondylus nicobaricus*	S.nicobaricus	W of New Briton, Papua New Guinea	EU379424	EU379478	EU379532	HM600743	UF322550
Spondylus wrightianus*	S.wrightianus	Stradbroke Island, QLD, Australia	KP300606	KP300571	KP300508	N/A	USC SCALLOG23
Swiftopecten swiftii	S.swiftii	Japan	KP300599	KP300565	KP300502	KP300532	Serb lab
Talochlamys multistriata	T.multistriata01	Raxo, Ria de Pontevedra, Gallicia, Spain	EU379403	EU379457	EU379511	HM630539	Serb lab
Talochlamys multistriata	T.multistriata02	Raxo, Ria de Pontevedra, Gallicia, Spain	HM630535	HM630536	HM630537	HM630538	Serb lab
Talochlamys tinctus	T.tinctus	Port Elizabeth, South Africa	HM630426	HM630427	HM630428	HM630429	UF329089
Talochlamys dichora	T.dichroa	Otago Peninsula, New Zealand	KP300577	KP300543	KP300480	KP300514	TM M297698
Talochlamys gemmulata	T.gemmulata	Stewart Island, New Zealand	KP300581	KP300547	KP300484	KP300517	TM M297697
Talochlamys pusio	T.pusio	Bergen, Norway	JQ611483	JQ611461	JQ611568	JQ611550	Genbank
Talochlamys pusio	T.pusio01	Raxo, Ria de Pontevedra, Gallicia, Spain	HM600764	HM600757	HM600737	HM600750	Serb lab
Verpichlamys empressae	V.empressae	Off Joga shima, Miura City, Japan	HM622673	HM622674	HM622675	HM622676	Serb lab
Verpichlamys jousseaumei	V.jousseaumei	Ktonan-cho, Japan	HM622710	HM622711	HM622712	HM622713	Serb lab
Verpichlamys kiwaensis	V.kiwaensis	Louisiville Ridge, New Zealand	KP300586	KP300552	KP300489	KP300521	NIWA TAN0707/84
Ylistrum balloti	Y.balloti	Bunderberg, QLD,	HM540088	HM540089	HM540090	HM540091	USNM

		Australia					1236641
Ylistrum japonicum	Y.japonicum	Oyano Island, Kumamoto, Japan	HM622706	HM622707	HM622708	HM622709	USNM 1236649
Zygochlamys amandi	Z.amandi	Puerto Montt, Chile	HM485575	HM485576	HM485577	HM485578	N/A
Zygochlamys delicatula	Z.delicatula	Dunedin, New Zealand	KP300576	KP300542	KP300479	KP300513	NIWA SCALNZ01
Zygochlamys patagonica	Z.patagonica	Chile	EU379412	EU379466	EU379520	HM630524	N/A

Table S3 Sensitivity simulations using different strengths of directional evolution (μ, from 2.1 to 3.5)**.** Angles (^{o}) shown are the mean pairwise angle (MPA) observed in the *Euvola* recessers (MPA-obs), and for the Brownian motion simulated data (MPA-BM) and Brownian motion plus directional trend data (MPA-BMT). In all cases, the observed pattern is more similar to those obtained under BM with a directional trend than to BM alone.

μ	MPA-obs	MPA-BMT	MPA-BM
3.5	41.5	36.42	60.15
3	41.5	41.02	60.13
2.75	41.5	43.64	60.15
2.5	41.5	46.29	60.16
2.25	41.5	49.56	60.16
2.1	41.5	51.55	60.12